

Resuspension bursts in particle-laden flows through porous media

Filippo Bianchi,^{1,*} Marcel Thielmann,^{2,†} and Hans Jürgen Herrmann^{1,‡}

¹*Computational Physics for Engineering Materials,*

Institute for Building Materials, ETH Zürich, 8093 Zurich, Switzerland

²*Bayerisches Geoinstitut, University of Bayreuth, 95440 Bayreuth, Germany*

We study particle-laden flows during deep bed filtration and show that in a specific range of fluid solid fractions the time evolution of pressure loss through the filter is characterized by distinct pressure jumps. These jumps stem from particle detachment events inside the porous medium and are preceded and followed by phases dominated by deposition. A statistical analysis shows that the events are independent of each other and their size distribution scales with a power law. The detection of these jumps is important to advance the understanding of particle-laden flows, which play an important role in a variety of fields, ranging from environmental sciences to industrial filters and petroleum recovery. Particularly, jumps are related to sand production in oil wells.

Depending on local flow conditions particle-laden flows through deep bed filters either deposit or detach material, having effects on permeability and pore structure.

Because of deposition, filters experience a porosity and permeability reduction, thus an increase of pressure gradient (in the case of constant flow conditions) [1–5]. Deposition mechanisms are particle interception by the filter matrix, inertial impaction of suspended particles against the matrix, brownian diffusion and gravity [4, 6, 7]. Upon contact with the filter matrix, suspended particles get caught on the filter matrix surface due to Van der Waals forces [4, 6, 7]. This process is particularly effective at small particle sizes ($<10^1 \mu\text{m}$). At larger particle sizes, mechanical clogging due to particle straining and bridge formation in pore throats is the main retention mechanism [6, 8].

Particle deposition is opposed by fluid flow induced drag forces. When the drag acting on a deposited particle exceeds the adhesive forces between the particle and the filter matrix or deposit, detachment occurs [9, 10]. Consequently, a critical fluid velocity (and thus a critical hydraulic gradient) is necessary to achieve particle resuspension [9, 11]. As flow surges increase fluid velocities, particle resuspension is enhanced if surges occur [12, 13]. Detachment is also favoured by instabilities caused by newly arriving suspended particles [14], which hit and detach previously deposited particles. Particles resuspended from the deposits can either be re-entrapped in deeper filter layers or exit the filter with the effluent [9, 15]. The former is more likely in the case of fine medium filters, where detachments are less probable [9]. The specific filter surface area increases with decreasing filter bed grain size, favouring adhesion of particles.

Changes in the porous medium morphology due to deposition modify particle detachment forces, as discussed in Ref. [16], which may overcome adhesive forces and resuspend previously deposited particles. Monte Carlo [17] and network models [18] of porous media have been developed to consider this effect. A thorough review of these models is found in Ref. [19]. When previously deposited particles are resuspended, porous media undergo a burst

in permeability, and an oscillatory behaviour between deposition and resuspension may occur (as observed in fractured carbonate oil reservoirs [20]). A precise analysis of such bursts is of great importance for a range of filtration-related applications such as the design of self-regenerating filters or the prediction of sand production in oil wells.

Here we present the results of a series of experiments where we investigated the deposition and resuspension processes in a granular deep bed filter. Experiments investigated the flow of a Newtonian aqueous suspension of quartz particles (whose size is large enough for Brownian motion to be negligible) through a densely packed filter bed of glass beads (see Fig. 7 for a sketch of the experimental setup and Appendix for details). The closed loop design of our setup allowed us to perform long-term experiments and thus to collect long data series. It also involves that the solid fraction of the suspension (ratio between volume of solid particles and total volume) at the filter inlet is coupled to the solid fraction at the outlet. Flow rate was varied from 0.2 to 0.5 ml/s, the solid fraction from $1.4 \cdot 10^{-3}$ to $1.3 \cdot 10^{-1}$. The same granular filter was used in all experiments. In a certain range of experimental parameters, we observed permeability jumps which can be related to particle resuspension bursts inside the filter body. These jumps exhibit distinct statistical properties. Scaling relations for both jump size as well as waiting time distributions are derived. Experiments with different filter type and suspension (see Appendix) also showed permeability jumps.

Effect of flow parameters on clogging behaviour of filter. The clogging behaviour of the filter is strongly influenced by solid fraction Φ and flow rates Q have a negligible effect (see Fig. 2). Three different regimes can be identified: a non-clogging regime, a clogging regime, and a transient regime in between.

At low solid fractions ($<10^{-2}$, green area in Fig. 2) pressure loss through the filter ($P = P_1 - P_2$, where P_1 and P_2 are the pressures at the filter inlet and outlet respectively) rises very slowly and asymptotically approaches a constant (see upper inset of Fig. 2 for typ-

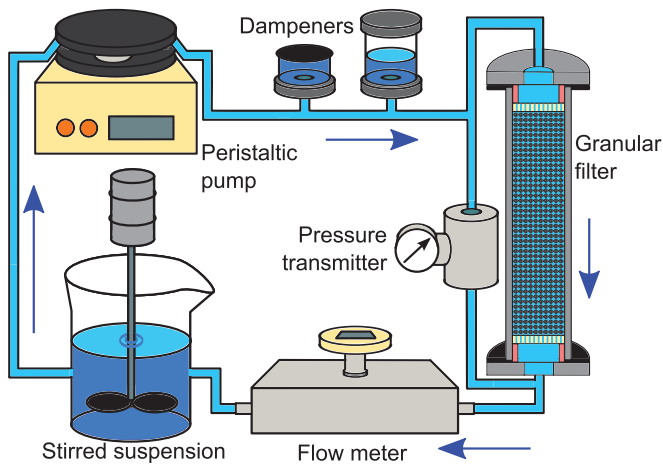


FIG. 1. Experimental setup. The suspension is pumped in a closed loop from a beaker through two pressure oscillation dampeners and through the granular filter. We measure pressure loss through the filter as well as volumetric and mass flow rates.

ical pressure loss vs. time t evolution). No significant fluctuations are observed, indicating that deposition does not play an important role and that particle detachment bursts are absent.

Experiments performed with a suspension solid fraction higher than 10^{-2} show a series of jumps in the pressure loss, thus in permeability. If Φ is below $4 \cdot 10^{-2}$, complete clogging does not occur (purple area of Fig. 2). The overall rise of pressure loss is very slow ($3 \cdot 10^4$ Pa in more than 4 days for the experiments shown in Fig. 3, which belong to the transient regime), meaning that the experiments are close to a steady state, in which the mean value of P neither increases nor decreases, but only fluctuates due to pressure loss jumps. This is an indication of a continuous competition between deposition and resuspension inside the filter.

If Φ is increased above $\simeq 5 \cdot 6 \cdot 10^{-2}$, pressure loss jumps are still observed during the experiments (brown area of Fig. 2, see lower inset for typical pressure loss vs. time evolution). In this case, the filter permeability reduction is so strong that complete clogging is reached and fluid flow in the system stops completely.

Solid fraction does have an effect on pressure loss jump size. In the transient regime, the average jump size is smaller than $3 \cdot 10^2$ Pa, whereas in the clogging regime the average jump size is larger than 10^3 Pa, even exceeding $8 \cdot 10^3$ Pa in cases close to the transient regime.

A dimensional evaluation of the parameters involved, reveals that the decline in filter permeability depends on the size of suspended particles [21]. Larger particle size results in a stronger decline in permeability under constant flow conditions. Particle strain also becomes relevant with increasing dimensionless ratio between the diameter of suspended particles and the diameter of the

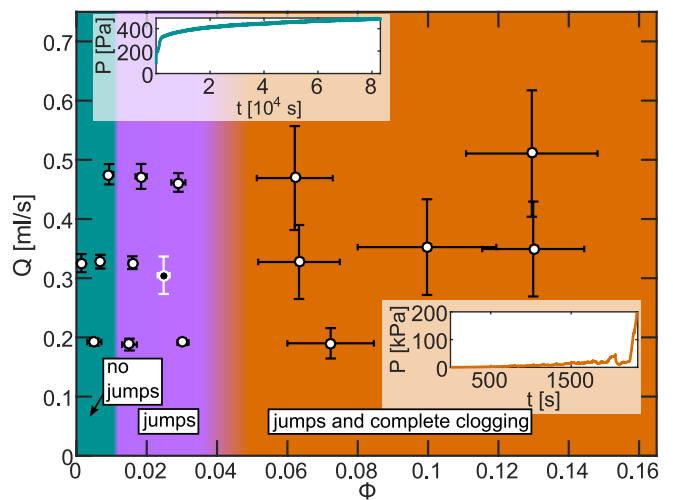


FIG. 2. Filter phase diagram. At low solid fractions the flux is continuous with no indications for clogging (green area). With increasing solid fraction, jumps are observed during the experiments, but the filter is not clogged (purple area). For even higher values of Φ , the filter reaches complete clogging (brown area). Every point in the diagram shows an experiment, error bars represent variations of Q and Φ during the experiment ($\pm 1.96\sigma$, σ is the standard deviation of data). The black point with white error bars indicates the parameters of the experiments subjected to a detailed analysis of jumps in the following of the paper. Insets show typical pressure loss vs. time evolution for experiments of non-clogging regime (upper inset) and clogging regime (lower inset).

matrix grains [6, 22]. Therefore the solid fraction thresholds reported are not universal, but vary depending on used suspensions and porous media. This was confirmed performing experiments with a different type of filter (with smaller size and porosity, see the Appendix for details) and suspension, which exhibit pressure loss jumps at lower solid fractions than those reported in Fig. 2.

Variation of Q does not have effects on filter clogging behaviour and only affects the time scale of pressure loss. Experiments run with high Q experience a faster rise in pressure loss, leading to an earlier occurrence of pressure loss jumps and the complete clogging of the filter.

Pressure loss jumps. Here we analyze three experiments that were run under the same experimental conditions and fall in the transient regime. The initial flow rate was set to 346 ± 2 $\mu\text{l/s}$, the initial suspension solid fraction was $3 \cdot 10^{-2}$. The time evolution of pressure loss through the experimental sample is shown in Fig. 3.

As shown in Fig. 3, the pressure loss through the filter increases with time, which can be attributed to particle deposition inside the filter (that reduces porosity and thus also permeability). The increase in pressure loss is not smooth, but rather characterized by jumps, during which the pressure loss is reduced.

Results show that pressure loss jumps occur only when P rises above 10^3 Pa (see Appendix for details). After

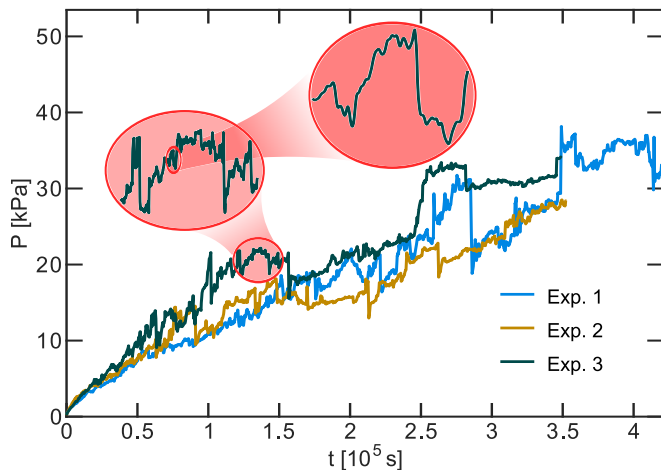


FIG. 3. Time evolution of pressure loss through the filter during three experiments. The time evolution of Q and Φ corresponding to the shown experiments is reported in Fig. 4.

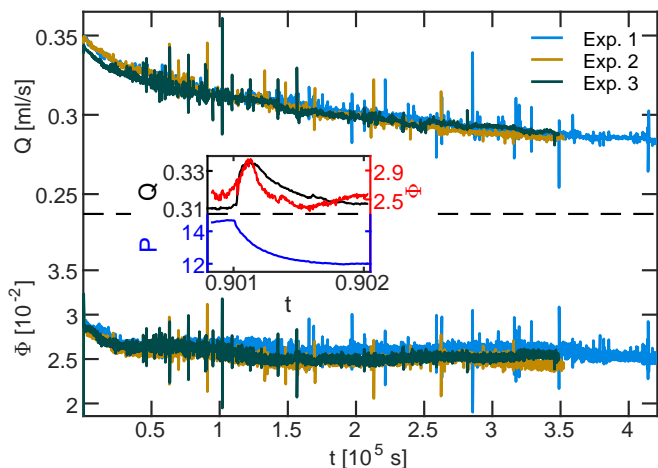


FIG. 4. Time evolution of flow rate and suspension solid fraction during the experiments of Fig. 3. The inset shows the evolution of flow rate and solid fraction (top), and pressure loss (bottom) during the jump of exp. 3 occurring at the time of $9 \cdot 10^4$ s (units are the same as in the main figure, pressure loss is in kPa).

reaching this value, jumps occur very frequently, with a recurrence time of $4\text{--}5 \cdot 10^2$ s.

Although peristaltic pumps are commonly assumed to produce a constant flow rate, their flow rate depends to some degree on the pressure loss through the system. We therefore also measured and report flow rate measurements, and show that pressure loss jumps coincide with high variations in flow rate (see Figs. 3 and 4). As shown in detail in the inset of Fig. 4, flow rate increases at the beginning of a jump until reaching a peak. Eventually it starts to decrease and approaches its initial value at the end of the jump. The suspension solid fraction at the filter outlet ($\Phi = (\rho - \rho_w) / (\rho_s - \rho_w)$, where ρ is

the suspension density, ρ_w the water density, and ρ_s the quartz density) also increases together with flow rate. It then decays faster than the flow rate to its initial level.

The fact that flow rate increases together with pressure loss jumps, indicates that sample permeability increases too. Since pressure jumps are related to increases in permeability and occur only after a critical pressure loss is reached (10^3 Pa), the jumps are due to particle resuspension events inside the granular medium. Local flow rates inside the filter during those events are so large that most detached particles are not redeposited, but flushed out of the filter. The permeability increase during the jumps can thus be explained by the opening of new channels.

The frequent occurrence of pressure loss jumps during experiments indicates that the experiments are characterized by a discontinuous interplay between deposition phases and detachment bursts. During periods of pressure loss increase, deposition dominates and pores in the filter become increasingly clogged. Consequently, local flow rates in the individual pores increase. As soon as the critical flow rate is reached in a pore, particle detachment occurs, resulting in the opening of the pore. Permeability then increases, while pressure loss and the local fluid velocity decrease, thereby restarting the cycle. An analogous phenomenon has been observed in the flow of acidic solutions through carbonate rocks [23–25], where the competition between dissolution and precipitation creates fluctuations in the rock permeability. Pressure loss jumps have also been recently observed in clogging of microchannels with colloidal particles [26–28].

Dependence of jump abruptness on jump size. We compute the jump abruptness as the ratio between jump size ΔP and its duration Δt_j . A linear trend appears in the log-log scale scatter graph showing the values of $\Delta P / \Delta t_j$ versus ΔP of all the data (see Fig. 5). Although there is a large scatter in the data, results are consistent in all three experiments and indicate that large jumps experience a faster decrease in pressure loss than small ones. A linear fit to the data suggests that jump abruptness scales with jump size to the power of 0.73 ± 0.03 ($\Delta P / \Delta t_j = 0.039 \Delta P^{0.73}$ is the straight line of Fig. 5, the error of the exponent represents the maximum difference between the fitted exponent of the data from all the experiments and the fitted exponent of data from a single experiment).

An explanation of this observation is given in the following. When a wide channel (or more channels at the same time) forms, the filter undergoes a substantial permeability increase. Consequently the pressure loss decreases significantly, resulting in a large jump. Vice versa, if a narrow channel is created the permeability increase will be limited and the related pressure loss jump smaller. A wide channel is also able to discharge fluid at a higher flow rate than a narrow channel, resulting in a faster drop in pressure loss for large jumps.

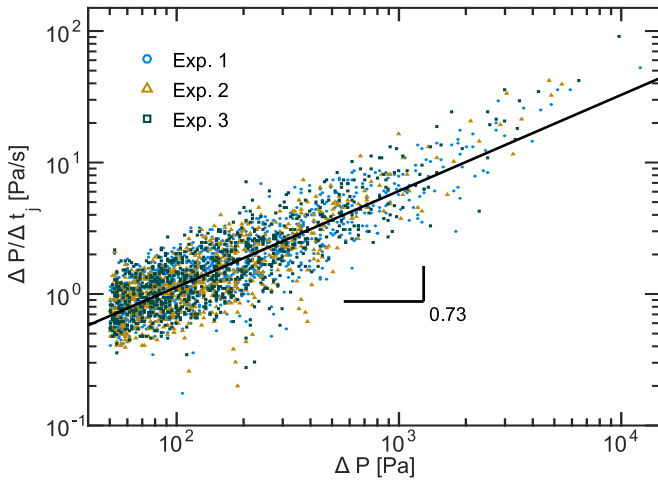


FIG. 5. Jump abruptness (ratio between jump size and time duration) vs. jump size. The black line is the linear fitting on log-log scale, whose slope is 0.73. Every point stems from a pressure loss jump.

Size distributions of jumps and waiting times. Jump sizes vary significantly during a single experiment (see Fig. 6). Minimal jump sizes correspond to the jump identification threshold ($5 \cdot 10^1$ Pa, see Appendix for details), while the largest jumps are about 10^4 Pa. Jump size exhibits a power law distribution with exponent $\alpha = 1.88 \pm 0.09$, indicating scale-invariant behaviour. α is computed using the maximum likelihood method [29], using data from all three experiments.

Waiting time distributions show a linear trend in a log-lin plot, indicating an exponential behaviour (upper inset in Fig. 6). When all three experiments are considered simultaneously, data is more scattered, resulting in a less accurate fit. The mean μ of the exponential distribution fitting all data is 313 ± 68 s. We thus deduce that pressure jumps are independent events, as in a Poisson process [30]. This point is also supported by the lack of correlations between jumps, which is deduced from the autocorrelation function of jump series (lower inset of Fig. 6).

Conclusion. The results of our experiments show that the clogging behaviour of a deep bed filter exhibits two basic regimes, namely the non-clogging regime and the clogging regime. While this well-known, our study is the first to closely investigate the transient regime between both end-members. This regime occurs only in a narrow band of suspension solid fractions, which complicates its detection. The transient regime is characterized by intermittency between deposition and resuspension phases. Deposition phases are characterized by a smooth pressure loss increase while resuspension phases appear as sudden events (pressure loss jumps). Both phases were analyzed with respect to their statistical properties. The abruptness of pressure loss jumps correlates with their size, with large pressure loss jumps being more abrupt than small

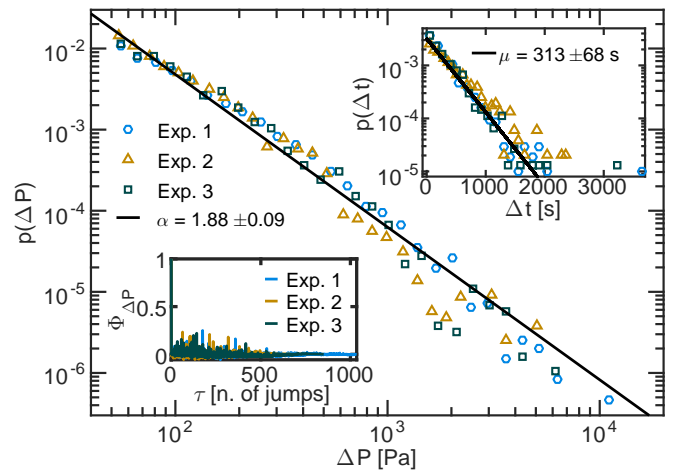


FIG. 6. Size distribution of pressure loss jumps. It exhibits power law behaviour with exponent $\alpha = 1.88 \pm 0.09$ (black line). The upper inset shows waiting times distributions. They are fitted with an exponential (black line), whose mean is 313 ± 68 s. The lower inset shows the autocorrelation function ($\Phi_{\Delta P}$) of pressure loss jumps (jump sizes in order of occurrence, τ is the lag). The error of the fitted parameters α and μ represents the maximum difference between the fitted parameters of data from all experiments and the fitted parameters of data from a single experiment.

ones. The size distribution of pressure loss jumps follows a power law distribution, while the waiting time distribution can be described by an exponential function. The exponential distribution of waiting times indicates that pressure loss jumps are independent events, which is also verified by analyzing the autocorrelation function.

The appearance of power law distributions is a common feature for phenomena exhibiting scale invariant behaviour. For instance, power laws are found in earthquakes [31, 32], solar flares [33, 34], stock markets [35, 36], and neural avalanches [37, 38]. The dynamics of these systems are characterized by the fact that they organize themselves into a critical state. The power law we found in jump size distribution suggests that also filtration processes, in the regime subjected to our investigation, attain a critical state.

Our experimental results are closely related to the model developed by Sampaio Filho et al. [39], which is based on the exact analogy between Ohm's and Darcy's laws and provides a possible description for particle-laden flows through porous media. In this model, temporal current fluctuations are observed, as a result of the switching of network links from insulator to conductor (and vice versa), when a critical voltage drop is reached. The resulting phase diagram exhibits three phases. A full metallic phase, where the network has its maximal conductance. An itinerant phase, in which conductance fluctuates. An insulating phase, where no current flows through the network. This phase diagram closely relates to the regime diagram presented in Fig. 2, which also

shows three regimes, one characterized by fluid flow and absence of jumps, one by intermittency between deposition and resuspension, and one in which the permeability reduces so strongly that fluid flux is inhibited.

Our experiments highlight the importance of particle resuspension during particle-laden flows through porous media. Our results are of particular interest for sand production in oil wells, a filtration scenario expected to occur in the transient regime. Sand avalanches in oil wells can be related to the resuspension events observed in our experiments. The presence of a power law size distribution implies that bursts have no characteristic size, thus avalanches of very large size can occur. Being uncorrelated events, large bursts can happen at any time. The phase diagram describing when resuspension bursts occur, is crucial to know under which conditions a system should be run to avoid resuspension. This is also relevant in the case of filtration of pollutants in soils, where resuspension bursts could release contaminants in the effluent.

The research leading to these results has received funding from the European Research Council, ERC Advanced Grant 319968-FlowCCS. We acknowledge the support of Falk K. Wittel and Claudio Madonna for helping in the design and realization of the experiments.

* fbianchi@ifb.baug.ethz.ch

† Marcel.Thielmann@uni-bayreuth.de

‡ hans@ifb.baug.ethz.ch

- [1] L. M. McDowell-Boyer, J. R. Hunt, and N. Sitar, *Water Resour. Res.* **22**, 1901 (1986).
- [2] J. L. Darby and D. F. Lawler, *Environ. Sci. Technol.* **24**, 1069 (1990).
- [3] J. R. Hunt, B. C. Hwang, and L. M. McDowell-Boyer, *Environ. Sci. Technol.* **27**, 1099 (1993).
- [4] C. Tien, *Principles of Filtration* (Elsevier, Amsterdam, 2012).
- [5] A. Alem, N.-D. Ahfir, A. Elkawafi, and H. Wang, *Transport Porous Med.* **106**, 303 (2015).
- [6] J. P. Herzig, D. M. Leclerc, and P. L. Goff, *Ind. Eng. Chem.* **62**, 8 (1970).
- [7] S. Ken, *Filters and Filtration Handbook* (Elsevier, Oxford, 2008).
- [8] J. R. Valdes and J. C. Santamarina, *SPE Journal* **11**, 193 (2006).
- [9] R. Bai and C. Tien, *J. Colloid Interf. Sci.* **186**, 307 (1997).
- [10] J. Bergendahl and D. Grasso, *Chem. Eng. Sci.* **55**, 1523 (2000).
- [11] A. Mahadevan, A. V. Orpe, A. Kudrolli, and L. Mahadevan, *EPL (Europhys. Lett.)* **98**, 58003 (2012).
- [12] S. Han, C. S. Fitzpatrick, and A. Wetherill, *Water Res.* **43**, 1171 (2009).
- [13] J. Kim and D. F. Lawler, *Water Res.* **46**, 433 (2012).
- [14] K. Ives, *Water Res.* **23**, 861 (1989).
- [15] J. Kim, , and J. E. Tobiason, *Environ. Sci. Technol.* **38**, 6132 (2004).
- [16] A. O. Imdakm and M. Sahimi, *Phys. Rev. A* **36**, 5304 (1987).
- [17] A. Imdakm and M. Sahimi, *Chem. Eng. Sci.* **46**, 1977 (1991).
- [18] M. Sahimi and A. O. Imdakm, *Phys. Rev. Lett.* **66**, 1169 (1991).
- [19] M. Sahimi, G. R. Gavalas, and T. T. Tsotsis, *Chem. Eng. Sci.* **45**, 1443 (1990).
- [20] M. Sahimi, A. R. Mehrabi, N. Mirzaee, and H. Rassamdana, *Transport Porous Med.* **41**, 325 (2000).
- [21] J. Moghadasi, H. Mller-Steinhagen, M. Jamialahmadi, and A. Sharif, *J. Pet. Sci. Eng.* **43**, 163 (2004).
- [22] M. Auset and A. A. Keller, *Water Resour. Res.* **42** (2006), 10.1029/2005WR004639, w12S02.
- [23] S. D. Rege and H. S. Fogler, *AIChE J.* **35**, 1177 (1989).
- [24] O. Singurindy and B. Berkowitz, *Water Resour. Res.* **39** (2003), 10.1029/2001WR001055, 1016.
- [25] O. Singurindy and B. Berkowitz, *Water Resour. Res.* **39** (2003), 10.1029/2002WR001624, 1143.
- [26] G. C. Agbangla, P. Bacchin, and E. Climent, *Soft Matter* **10**, 6303 (2014).
- [27] Z. B. Sendekie and P. Bacchin, *Langmuir* **32**, 1478 (2016).
- [28] Z. B. Sendekie, A. Gaveau, R. G. H. Lammertink, and P. Bacchin, *Sci. Rep.* **6**, 31471 (2016).
- [29] M. E. J. Newman, *Contemp. Phys.* **46**, 323 (2005).
- [30] E. Parzen, *Stochastic Processes* (Society for Industrial and Applied Mathematics, Philadelphia, 1999).
- [31] B. Gutenberg and C. F. Richter, *B. Seismol. Soc. Am.* **34**, 185 (1944).
- [32] L. de Arcangelis, C. Godano, J. R. Grasso, and E. Lippiello, *Phys. Rep.* **628**, 1 (2016).
- [33] E. T. Lu and R. J. Hamilton, *Astrophys. J.* **380**, L89 (1991).
- [34] M. Mendoza, A. Kaydul, L. de Arcangelis, J. S. Andrade Jr, and H. J. Herrmann, *Nat. Commun.* **5**, 5035 (2014).
- [35] P. Gopikrishnan, V. Plerou, X. Gabaix, and H. E. Stanley, *Phys. Rev. E* **62**, R4493 (2000).
- [36] M. Bartolozzi, D. Leinweber, and A. Thomas, *Physica A* **350**, 451 (2005).
- [37] J. M. Beggs and D. Plenz, *J. Neurosci.* **23**, 11167 (2003).
- [38] L. de Arcangelis and H. J. Herrmann, in *Criticality in Neural Systems*, edited by D. Plenz and N. Ernst (Wiley-VCH Verlag GmbH & Co. KGaA, Weinheim, 2014) pp. 273–292.
- [39] C. I. N. S. Filho, A. A. Moreira, N. A. M. Araújo, J. S. Andrade, and H. J. Herrmann, *Phys. Rev. Lett.* **117**, 275702 (2016).

APPENDIX A: EXPERIMENTAL SETUP

The aqueous suspension used in the experiments is composed of deionized boiled water and quartz powder (> 230 mesh, Sigma Aldrich). The d_{50} of quartz particles is 25 μm . The granular packing constituting the filter consists of soda lime glass beads (Sigmund Lindner) with a diameter of 0.9 to 1 mm. The granular packing is embedded in an aluminium cylinder (height 80 mm, diameter 16 mm). A peristaltic pump (Gilson MINIPULS 3), controlled via computer through an I/O module (Meilhaus Electronic RedLab 1208LS), pumps

the fluid through the granular packing. Pressure oscillations generated by the pump are dampened by a combination of a neoprene membrane dampener and an air chamber. The pressure loss through the experimental sample is measured with a differential pressure transmitter (Keller PRD-33 X, ± 145 Pa accuracy). A Coriolis flow meter (Endress+Hauser Proline Promass A 100) is placed at the sample outlet to measure volumetric (± 0.4 $\mu\text{l/s}$ accuracy) and mass (± 0.6 mg/s accuracy) flow rates. It allows for the calculation of the suspension solid fraction (Φ), as the volumetric (Q) and mass (\dot{M}) flow rates, water density ($\rho_w = 998.4 - 999.4$ kg/m³), and quartz density ($\rho_s = 2648$ kg/m³) are known ($\Phi = (\rho - \rho_w) / (\rho_s - \rho_w)$, where $\rho = \dot{M}/Q$ is the suspension density). The flow meter is connected to a PC via a DAQ device (Meilhaus Electronic RedLab 1208FS).

APPENDIX B: SAMPLE PREPARATION AND EXPERIMENTAL PROCEDURE

To prepare the sample for the experiments, a 3D printed polycarbonate sieve (3 mm height) was positioned at the lower side of the aluminum cylinder. A rubber ring (6 mm height), placed below the sieve held it in place. The cylinder was then filled with glass beads (20 ± 0.05 g), placed on a vibrating table (a loud speaker connected to an oscilloscope) and vibrated at 150 Hz for 30 s. Lids were fastened to the cylinder after also placing a polycarbonate sieve and a rubber ring on the upper end. A seal was created by neoprene rings positioned between the lids and the cylinder. The grains were compressed by the polycarbonate filters and the rubber rings, to ensure packing rigidity.

The sample was initially filled with clean water. Air bubbles were removed by flushing the sample in both directions with water at flow rates of $\simeq 0.7$ ml/s, while simultaneously shaking it vigorously. Upon removal of all air bubbles, the quartz powder was added to the water and the experiment started at the desired flow rate. During the whole experiment, the pressure loss through the sample, the volumetric flow rate, and the mass flow rate were recorded at a sampling rate of 2 Hz. At the end of the experiment, the sample was cleaned with deionized water. We produced many samples but all the experiments reported in the letter were run with the same bead packing.

APPENDIX C: SECOND TYPE OF FILTER

We also ran a set of experiments using a different type of granular filter and suspension. The filter consists in this case of sintered soda-lime glass beads (200-300 μm of diameter, Sigmund Lindner), it has a cylindrical shape (length $\simeq 14$ mm, diameter $\simeq 5.5$ mm), and a porosity

of 0.17-0.23. The suspension used is composed of SiO₂ particles (0.5-10 μm diameter, Sigma Aldrich), at solid fractions of $5.3-7.5 \cdot 10^{-4}$. We used the same experimental setup as previously described, replacing the flow meter by a Sensirion SLQ-QT500 (accuracy 5 % o.r.). Flow rates used in the experiments ranged between 0.1 and 0.2 ml/s. Due to the impossibility of cleaning the filter after each experiment, every experiment had to be run with a new filter.

An example of pressure loss evolution in an experiment run with this type of filter is shown in Fig. 7.

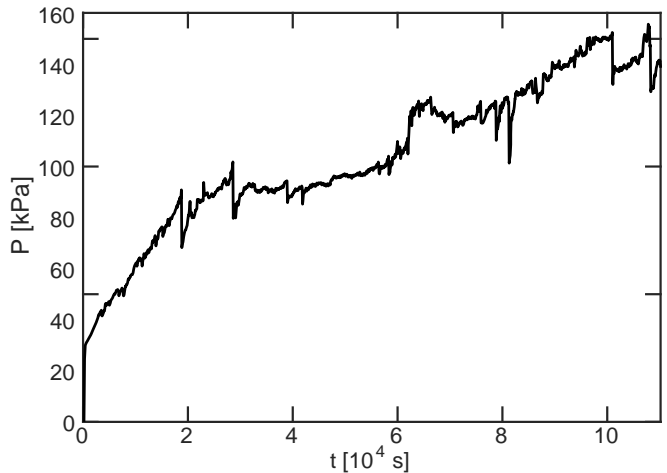


FIG. 7. Time evolution of pressure loss through the sintered filter. The solid fraction of suspension is $6 \cdot 10^{-4}$, the initial flow rate is 0.16 ml/s.

APPENDIX D: DATA POSTPROCESSING: IDENTIFICATION OF JUMPS

Time series of the pressure loss were filtered with a second order low-pass Butterworth filter with a cutoff frequency of 0.015 Hz to remove experimental noise (instrumentation noise and pump pulsations). Pressure loss jumps are then detected in the filtered data. The size of those jumps (ΔP) is computed as the pressure loss difference between a local maximum and the following local minimum. Jumps with sizes smaller than 50 Pa were neglected as their amplitude is smaller than the noise amplitude.

APPENDIX E: JUMP SIZE DISTRIBUTION

Depending on the minimum threshold used to recognize jumps, a deviation from the power law distribution may appear for smallest jump sizes ($< 5 \cdot 10^1$ Pa). Such jumps would be smaller than the noise due to the experimental apparatus (oscillations coming from the peri-

staltic pump) experienced at the end of an experiment. We thus decided to neglect them.